JACS
JOURNAL OF THE AMERICAN CHEMICAL SOCIETY
pubs.acs.org/JACS
Article

Electrochemical Reduction of Perfluorooctanoic Acid (PFOA): An Experimental and Theoretical Approach

Jonathan J. Calvillo Solís, Christian Sandoval-Pauker, David Bai, Sheng Yin, Thomas P. Senftle, and Dino Villagrán*

Cite This: J. Am. Chem. Soc. 2024, 146, 10687−10698
Read Online
ACCESS | Metrics & More | Article Recommendations | Supporting Information

ABSTRACT: Perfluorooctanoic acid (PFOA) is an artificial chemical of global concern due to its high environmental persistence and potential human health risk. Electrochemical methods are promising technologies for water treatment because they are efficient, cheap, and scalable. The electrochemical reduction of PFOA is one of the current methodologies. This process leads to defluorination of the carbon chain to hydrogenated products. Here, we describe a mechanistic study of the electrochemical reduction of PFOA in gold electrodes. By using linear sweep voltammetry (LSV), an $E^{0\prime}$ of −1.80 V vs Ag/AgCl was estimated. Using a scan rate diagnosis, we determined an electron-transfer coefficient (α_{exp}) of 0.37, corresponding to a concerted mechanism. The strong adsorption of PFOA into the gold surface is confirmed by the Langmuir-like isotherm in the absence ($K_A = 1.89 \times 10^{12}$ cm^3 mol^{-1}) and presence of a negative potential ($K_A = 3.94 \times 10^7$ cm^3 mol^{-1}, at −1.40 V vs Ag/AgCl). Based on Marcus−Hush's theory, calculations show a solvent reorganization energy (λ_0) of 0.9 eV, suggesting a large electrostatic repulsion between the perfluorinated chain and water. The estimated free energy of the transition state of the electron transfer ($\Delta G‡ = 2.42$ eV) suggests that it is thermodynamically the reaction-limiting step. $^{19}F - {}^{1}H$ NMR, UV−vis, and mass spectrometry studies confirm the displacement of fluorine atoms by hydrogen. Density functional theory (DFT) calculations also support the concerted mechanism for the reductive defluorination of PFOA, in agreement with the experimental values.

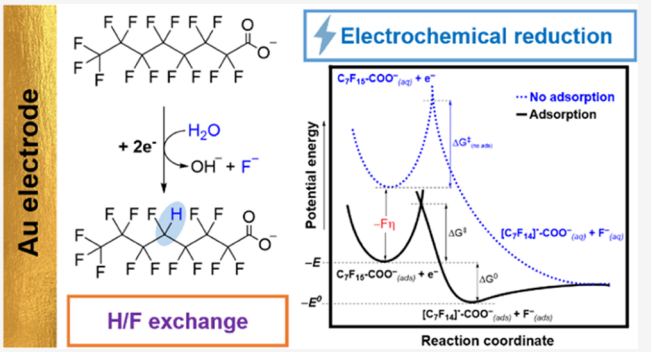

INTRODUCTION

Poly- and per-fluoroalkyl substances (PFAS) are a family of artificial molecules with total or partially fluorinated carbon chains.[1] The amphipathic nature of PFAS by the hydrophobic alkyl and the hydrophilic functional group (e.g., R−OH, RSO_3^-, $RCOO^-$) gives them exceptional surface properties as surfactants.[2,3] The strong C−F bond energy (459.8 kJ mol^{-1})[4] makes them highly stable to thermal and chemical decomposition under typical environmental conditions.[5] For this reason, since the 1940s, PFAS have been utilized in several areas, such as medicine, industry, paint production, aqueous film-forming foams (AFFF), and food packaging and processing,[6−8] causing its wide distribution in soil, water, food, and living organisms (animals, plants, and humans).[9] However, the PFAS presence in water is an important environmental concern because they are easily bioaccumulated and are highly toxic even at low concentrations.[10−12]

An important group of PFAS is the perfluorocarboxylic acids (PFCAs), in which perfluorooctanoic acid (PFOA) has the most severe environmental concern.[13] Several strategies have been adopted to remove and destroy PFOA from water. Electrochemical methods are getting attention due to their versatility, low cost, and high removal efficiencies, and they are environmentally friendly because they can be powered by renewable energy.[14,15] The carboxylic group available in the PFOA chain can be anodically oxidized according to the Kolbe decarboxylation,[16] in which the CO_2 leaving produces a free radical intermediate that can interact with other reactive species (such as $^{\bullet}OH$) to produce a molecule easier to oxidize.[17] The continuous removal of CO_2 from the chain causes the PFOA to break down, resulting in shorter chains and the release of F^- ions. For this reason, electrochemical oxidation is a viable method as water treatment,[6,18,19] frequently done with boron-doped diamond[20] and TiO_2 electrodes.[21] Recent work has emphasized electrochemical reduction as an alternative strategy for the remediation of water contaminated with PFAS.[3,22−25] The methodology is

Received: January 11, 2024
Revised: March 19, 2024
Accepted: March 20, 2024
Published: April 5, 2024

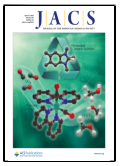

https://doi.org/10.1021/jacs.4c00443
J. Am. Chem. Soc. 2024, 146, 10687−10698

based on substituting fluorine atoms with hydrogen atoms. In the process, the formation of totally or partially hydrogenated chains has been reported, transforming the PFOA molecule into partially hydrogenated species with lower environmental concern.[26] For example, the complete reduction of PFOA (C_7F_{15}−COOH) produces octanoic acid (C_7H_{15}−COOH). However, this transformation is often incomplete due to the significant amount of energy required to substitute all of the fluorine atoms. Therefore, it is common to obtain partially hydrogenated byproducts. Nonetheless, this mechanism has not been explained in depth, nor has the electrochemical behavior of PFOA been fully studied.

In this work, we have followed the electrochemical reduction of alkyl halides as a model to explain the reduction of PFOA. This mechanism consists of a dehalogenation process based on dissociative electron-transfer (DET) theories[27] aiming to explain how the C−X bond splits through an electron-transfer (ET) reaction. Two possible pathways have been studied, stepwise or concerted mechanisms, in which ET and bond breaking occur in single or multiple steps.[28] In both pathways, two electrons are involved. As shown in Scheme 1, the stepwise

Scheme 1. Two Possible Mechanisms Proposed For Reduction of Alkyl Halides

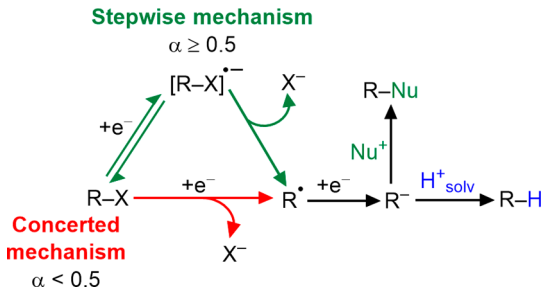

mechanism leads to the intermediate formation of a radical anion $[R–X]^{\bullet-}$ of the corresponding halide. Once the $[R–X]^{\bullet-}$ is electrogenerated, the C−X bond splits immediately to form a free radical $R^{\bullet}$.[29,30] Further, the reduction potential of the $R^{\bullet}$ radical is generally more positive than that of the initial halide, so it is rapidly reduced to the corresponding carbanion R^-. The concerted pathway leads to the formation of an $R^{\bullet}$ radical and an X^- anion directly.[28,30] Eventually, the R^- species can subtract a hydrogen proton from the solvent[31] and perform a nucleophilic attack if any nucleophile is available.[32] The dehalogenation mechanism depends on the nature of the electrode material, the target organic halide, the solvent, and the availability of protons in the reaction medium.[27,32,33] The nature of both mechanisms lies in the kinetics and thermodynamics of DET.[28]

The reduction of PFOA is challenging because more negative potentials are required, and it is often not possible because water reduction occurs first by its less negative potential. Therefore, this reaction interferes even at alkaline pH (eq 1).

$$2H_2O + 2e^- \rightleftarrows H_2 + 2OH^- \quad E^0 = -0.83\,\text{V vs SHE} \tag{1}$$

To reduce the overpotential of PFOA reduction and minimize water reduction interference, electrodes made of noble metals such as Au and Ag were used. We present an electrochemical and an NMR characterization and a computational study to explore the reduction of PFOA in aqueous media. Using the Marcus−Hush approach, we study the reorganization effects during the electron-transfer reaction and explain how other factors (such as adsorption) are involved in this electrochemical reaction.

MATERIALS AND METHODS

Materials. The reagents employed were of analytical grade. Perfluorooctanoic acid (PFOA, 95%) was obtained from Sigma-Aldrich. The electrolyte support was $KHCO_3$ (99%) from Fisher Scientific. The solutions were prepared using ultrapure water (18 MΩ).

Instrumentation. All electrochemical experiments were performed at 20 ± 2 °C in an electrochemical cell with a three-electrode arrangement connected to a CHI760D potentiostat. The reference electrode was Ag/AgCl in a 1 M KCl aqueous solution, and a platinum mesh was used as the auxiliary electrode. The working electrodes were 3 mm diameter gold, silver, and glassy carbon (GC) purchased from CH Instruments. The 3 mm diameter boron-doped diamond (BDD) was acquired from BioLogic USA. Before each experiment, the working electrodes were carefully polished on a cloth-polishing pad for 1 min using 0.30 and 0.05 μm alumina slurry. Later, the electrodes were cleaned by ultrasonication for 2 min in DI water, ethanol, and acetone and dried under an N_2 atmosphere for 2 min. The gold electrode was then cleaned electrochemically in a 0.5 M H_2SO_4 solution using a window potential from 0.40 to 1.60 V vs Ag/AgCl. Cycling was done until a stable peak current was observed in the typical cyclic voltammogram for gold.

Preparative Bulk Electrolysis and NMR Characterization. Controlled-potential electrolysis (CPE) was performed in an electrochemical h-cell. In the cathodic cell, 1 mM PFOA + 0.5 M $KHCO_3$ (pH 9.5) was added. In the anodic cell, 0.5 M $KHCO_3$ was added. A gold electrode (area: 0.196 cm^2) was used as a cathode, and a TiO_2 mesh (area: 6 cm^2) was used as an anode. The potential applied was Ep_c − 150 mV. The bulk electrolysis was carried out under constant stirring and an N_2 atmosphere to avoid oxygen interference. Faraday's law determined the number of transferred electrons (n_{exp}) from the experimentally obtained charge (Q_{exp}).

The PFOA and the working solution were analyzed in a Bruker Advance III 400 MHz NMR Spectrometer. ^{19}F NMR spectrum was acquired using 500 scans with a recycle delay of 30 s. Hexafluorobenzene (HFB) was used as the external standard at −164.9 ppm,[34] and the spectra obtained were referenced to this signal. In a 5 mm glass NMR tube, 200 μL of 1 mM PFOA, 10 μL of HFB, and 100 μL of deuterium oxide (D_2O) were added as a signal locking solvent. The same quantities were employed for the electrolysis reaction solution. A ^1H NMR spectrum was acquired using 16 scans with a 1 s recycle delay. In a 5 mm glass NMR tube, the PFOA and the hydrogenated compounds (from the bulk electrolysis) were extracted *in situ* by a liquid−liquid extraction by adding 200 and 800 μL of $CDCl_3$ (99.8% D atom, Sigma-Aldrich). The aqueous phase was removed before NMR analysis. Phase angle, baseline correction, and integration were performed manually.

Quantification of F^- Ions by a Fluoride Ion-Selective Electrode (F−ISE). A solid-state ion-selective electrode (ISE) with a lanthanum fluoride crystal membrane from Hanna Instruments (HI-4110) was used for the quantification of fluoride ions in an aqueous solution. The pH and ionic strength of the samples were adjusted to a constant value by adding the total ionic strength adjustment buffer (TISAB, Hanna Instruments) to ensure that the solution pH was between pH 5 and 8. The F^- ions analysis was done following the EPA-approved ISE test procedures ASTM D1179-04 for F^- ions in drinking water.

UV−Vis Spectroscopy. The measurements were performed on a SHIMADZU UV−3600 Plus Spectrophotometer. A 0.5 M $KHCO_3$ solution (pH 9.5) was used as a blank.

Mass Spectroscopy. The analysis of the PFOA and bulk electrolysis products was performed on a JEOL JMS-T100LC mass spectrometer. The spectra were obtained in the mass-to-charge ratio

https://doi.org/10.1021/jacs.4c00443
J. Am. Chem. Soc. 2024, 146, 10687−10698

(m/z) range from 250 to 450 in the negative ionic mode. Parameters for the mass spectrometer were as follows: ions source gas 1, temperature, 321 °C; ion spray voltage floating, −500 V; collision energy, −10 V; declustering potential, −100 V.

Computational Details. Calculations were performed using density functional theory (DFT), as implemented in the ORCA program package v.5.0.3.[35] All structures were optimized in the solvent phase using the meta GGA hybrid TPSSh functional combined with the def2-TZVP basis set.[36−38] Grimme's D3 protocol combined with the Becke−Johnson (D3BJ) damping scheme was employed to include dispersion effects in all calculations.[39] A tight convergence (energy change, TolE = 1×10^{-8}; RMS density change, TolRMSP = 5×10^{-9}; maximum density change, TolMaxP = 1×10^{-7}; DIIS error convergence, TolErr = 5×10^{-7}) of the wave function and a grid quality defgrid2 were requested. To accelerate the DFT calculations, we employed the resolution of the identity approximation for Coulomb and chain of spheres approximation for exchange interactions (RIJCOSX).[40]

Geometry optimizations were followed by the calculation of numerical vibrational frequencies in the solvent phase at the same level of theory as optimization calculations (TPSSh-D3/def2-TZVP/defgrid2) to evaluate that the optimized equilibrium structures correspond to minima of the potential energy surface and to obtain the thermodynamic corrections via the rigid-rotor and harmonic oscillator approximations at T = 273.15 K. The universal solvation model based on solute electron density (SMD),[41] as implemented in Orca 5.0.3, was employed to account for the solvent effects. The GEPOL algorithm[42−44] generated the solvent cavity as a solvent-excluded surface. The atomic radii of the default method were adjusted to H (1.250 Å), C (2.000 Å), O (1.600 Å), and F (1.682). The radius of water was set at 1.40 Å.

For the computation of reduction potentials, we employed the defining equation of the half-cell potential of an A/A^- redox couple (eq 2) where $\Delta G^{0,sol}$ corresponds to the solution-state reaction Gibbs free energy of the reduction process, n is the number of electrons transferred (n = 1), and F is the Faraday constant (F = 96,485 C mol^{-1}). The standard reduction potential (E^0) was determined from the half-cell potential minus the absolute half-cell potential of the reference electrode, SHE (4.44 V).[45]

$$E_{1/2}(A/A^-) = \frac{-\Delta G^{0,sol}(A/A^-)}{nF} \quad (2)$$

Multiwfn[46] software v. 3.8 was used to perform the electron density difference ($\Delta\rho$) map of PFOA. Orbitals and the $\Delta\rho$ map were visualized and plotted in VMD 1.9.3.[47] More details about the computational methods and procedures are provided in the Supporting Information (SI).

RESULTS AND DISCUSSION

PFOA is a stable compound that is difficult to reduce. At the large potential required for PFOA reduction, hydrogen evolution (HER) is an interfering reaction. HER can be minimized by using alkaline media, as its reduction potential is shifted toward more negative potentials as the pH increases.[48]

Our first objective was to identify a PFOA reduction peak using linear sweep voltammetry (LSV). For this, an alkaline blank solution of 0.5 M $KHCO_3$ was studied at pH 9.5. Figure 1a shows the polarization curve of the blank solution using gold, silver, glassy carbon (GCE), and boron-doped diamond (BDD) electrodes. The gold electrode (black line) has the largest water reduction activity compared to silver, glassy carbon, and BDD. The gold electrode shows the smallest water reduction overpotential, followed by silver, glassy carbon electrode (GCE), and finally, BDD. In the presence of PFOA (Figure 1b), no new peak is observed when using BDD, and a very small shoulder increase is observed with GCE. This suggests that a larger overpotential is required compared to the

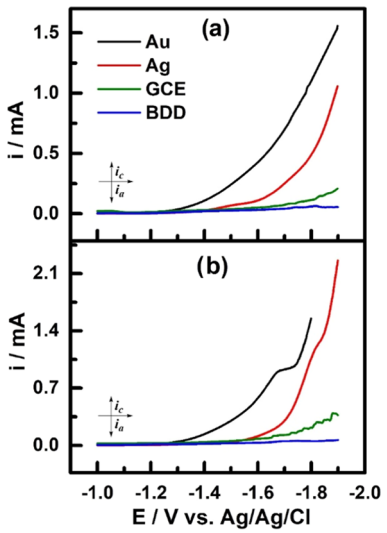

Figure 1. LSV response of Au, Ag, glassy carbon (GC), and boron-doped diamond (BDD) electrodes. (a) Blank signals in 0.5 M $KHCO_3$. (b) Response of 1 mM PFOA. pH 9.5, v = 50 mV s^{-1}, φ = 3 mm.

gold or silver electrodes. Therefore, these electrodes are inert to PFOA reduction. However, a new shoulder peak appears with the gold and silver working electrodes at peak potentials (Ep_c) of −1.68 and −1.82 V vs Ag/AgCl, respectively. At the silver electrode, the peak is weakly defined, and this signal disappears after cycling the electrode (10 runs) between −1.00 and −1.80 V vs Ag/AgCl (Figure S1). This signal also vanishes upon stirring. These observations suggest that this peak arises from capacitive current due to the adsorption of PFOA into the surface of the silver electrode and not due to its reduction.[49,50] The signal at −1.68 V observed with the gold working electrode is stable and did not disappear after several runs or upon stirring. The mass transport zone is observed between −1.68 and −1.75 V before the water reduction current starts to increase again. Therefore, it is possible to identify the reduction of PFOA even with constant competition against the electrochemical reduction of water.

Optimization of the pH in the range of 6.0 to 11.0 was studied using a gold electrode. As shown in Figure S2a, PFOA is completely deprotonated to the carboxylate anion after pH 6, considering its pK_a is 3.8.[51] LSV measurements performed at different pH values (Figure S2b) show that the change in Ep_c is not Nerstian (i.e., Ep_c is not linear at different pH values). At pH values below 6.0, the PFOA peak was not observed because it was outperformed by HER. Electrogenerated hydrogen bubbles likely promote PFOA desorption, which hinders its reduction. The absence of the peak between pH 6.0 and 8.0 suggests that water reduction predominates over PFOA reduction. The reduction event of the PFOA peak is observed after more basic conditions (pH > 9.0), with an optimized and stable LSV response at pH 9.5. For this reason, this pH was used for the following experiments.

The PFOA adsorption into the four different electrode materials was studied by square-wave voltammetry (SWV). PFOA molecules are expected to adsorb onto the surfaces through electrostatic interactions.[52] The adsorbed PFOA concentration can be quantified from the decrease in the Faradaic current of a redox probe such as $[Fe(CN)_6]^{3-/4-}$ and renders the active sites of the electrode electrochemically

https://doi.org/10.1021/jacs.4c00443
J. Am. Chem. Soc. 2024, 146, 10687−10698

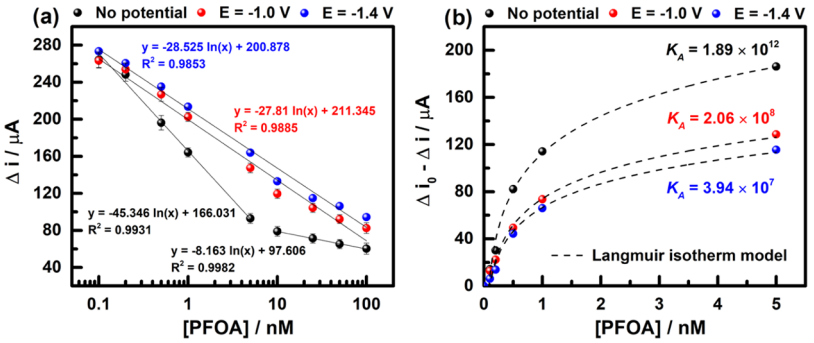

Figure 2. (a) Dependence of the SWV response on PFOA concentration for an Au electrode immersed by 4 h under free potential conditions and at $E = -1.00$ V and $E = -1.40$ V vs Ag/AgCl. (b) Fitting of the experimental data with the Langmuir isotherm model.

inactive. The electrodes were immersed in a 100 nM PFOA solution for 16 h to ensure adsorption equilibrium. Figure S3a shows the square-wave responses (Δi) of the four electrodes. The Δi decreases with time until it remains constant. For the silver and gold electrodes, the equilibrium is reached at 4 h. Meanwhile, for glassy carbon and BDD electrodes, the equilibrium is achieved after 8 h. Therefore, we selected an equilibrium time of 4 h for gold and silver and 8 h for GC and BDD electrodes to measure the adsorption constant (K_A). A modified Langmuir isotherm model, as described in eq 3, was used to measure K_A:

$$\Delta i_0 - \Delta i = \frac{\Delta i_0 [\mathrm{PFOA}] K_A}{1 + [\mathrm{PFOA}] K_A} \quad (3)$$

where Δi_0 is the square-wave current of the free-PFOA electrode, Δi is the response of the electrode with PFOA adsorbed at a specific concentration, and K_A is the adsorption constant in $cm^3\ mol^{-1}$.[53] As shown in Figure S3b, the square-wave current changes for the $[Fe(CN)_6]^{3-/4-}$ redox probe; as the electrode surface becomes saturated with PFOA, the active surface area decreases as a function of the ln [PFOA]. Figure S3c shows the fit of the experimental data to the Langmuir isotherm model. The K_A value for glassy carbon, BDD, Ag, and Au electrodes is 4.16×10^{10}, 2.57×10^5, 1.16×10^{12}, and 1.89×10^{12} $cm^3\ mol^{-1}$, respectively. The results show that PFOA adsorption is more thermodynamically favorable on gold and silver surfaces than in glassy carbon and BDD electrodes. To assess the effect of the negative potential applied during the reduction reaction on the PFOA adsorption, we performed the same measurements applying a potential of −1.00 V vs Ag/AgCl. Figure S4 shows the fit of the experimental data to the Langmuir isotherm model. The K_A value for glassy carbon, BDD, Ag, and Au electrodes is 8.26×10^3, 0.34, 5.75×10^5, and 2.06×10^8 $cm^3\ mol^{-1}$, respectively. The equilibrium constants at negative potentials show a weakening of the PFOA interactions into the glassy carbon, BDD, and Ag electrodes. The difference in magnitude between the K_A values with and without an applied potential of the different electrodes suggests that gold surfaces have an affinity toward PFOA adsorption, and we hypothesize that this preference has important effects on the kinetics and thermodynamics of electron transfer.

The adsorption of PFOA into a gold surface was studied in depth in the absence and presence of a negative potential. In the absence of potential, two linear regions are observed (Figure 2a, see black spheres). The first region is defined from 0.1 to 5 nM and the second region from 10 to 100 nM. Both ranges follow a Langmuir-like adsorption behavior. The first range shows a sigmoidal shape following the behavior of the Langmuir isotherm model. The fact that two linear regions were observed suggests that the PFOA distribution throughout the surface is not homogeneous because multiple approaches to PFOA adsorption exist beyond the ideal monolayer adsorption of the Langmuir isotherm.[54] In the low-concentration region (0.1−5.0 nM), the PFOA molecules are adsorbed at a random orientation along the electrode surface. At higher concentrations of PFOA (10−100 nM), the electrostatic repulsions between the PFOA molecules promote a "heads-on" type orientation to minimize adsorbate−adsorbate interactions.[55]

Under a potential of −1.00 V versus Ag/AgCl, we immersed the gold electrode in PFOA solutions of 0.1, 5, and 100 nM for 16 h to ensure adsorption equilibrium. Figure S5 shows the square-wave responses (Δi) of the Au electrode. The equilibrium is reached at 4 h in all of the concentrations. The above data suggest that the adsorption kinetics of PFOA under negative potential is not influenced by the concentration. At a potential of −1.00 and −1.40 V (Figure 2a, see red and blue spheres), only one region is observed along the concentration range. This suggests that PFOA adopts only one orientation. Figure 2b shows the fit of the experimental data to the Langmuir isotherm model. At a potential of −1.00 and −1.40 V, the K_A are 2.06×10^8 $cm^3\ mol^{-1}$ and 3.94×10^7 $cm^3\ mol^{-1}$, respectively. The decrease of K_A by four and five orders of magnitude compared to the K_A determined in the absence of a potential shows that the negative charge of the electrode promotes the partial desorption of PFOA. A similar behavior is observed in the electrochemical active surface area (ECSA). As shown in Figure S6, we calculated the double-layer capacitance (C_{dl}) and, subsequently, the ECSA values (Table S1). The bare gold electrode, in the absence of a negative potential, shows an ECSA of 5.31 cm^2. Once PFOA is adsorbed on the surface, the ECSA decreases to 3.07 cm^2, which shows the coverage of the electrode by the PFOA molecules. At $E = -1.4$ V, the surface area increases to 3.77 cm^2, which confirms the strong adsorption of PFOA into the gold electrode. We proposed that PFOA acquires a "tails-on" orientation in which the perfluorinated chain interacts with the electrode surface in a horizontal position. In this orientation, electrostatic repulsions between the PFOA carboxylate groups on the surface may weaken the adsorption.[54] This orientation may also facilitate electron transfer to the C−F bonds proximal to the electrode surface, as it has been previously reported.[54]

To determine the mass transport of the reaction and to obtain information on the kinetics and thermodynamics of the

https://doi.org/10.1021/jacs.4c00443
J. Am. Chem. Soc. 2024, 146, 10687−10698

electron-transfer processes, we measured the scan rate (ν) effect on the reduction of PFOA in the range from 50 to 200 mV s^{-1} for the Au electrode (Figure S7a). Figure S7b shows the proportional increase of the cathodic peak current (ip_c) with respect to ν (ip_c = 2113.493 ν − 66.833, R^2 = 0.995), which corresponds to an adsorption-controlled mass transport mechanism. Plotting the log ip_c vs log ν (Figure S7c) shows a linear tendency (log ip_c = 0.975 log ν + 3.707, R^2 = 0.988) with a slope close to 1.[56] These results confirm that PFOA adsorption is more favorable than mass transport by diffusion. The plot of Figure S7d shows a shift of Ep_c toward more negative potentials as the scan rate increases (Ep_c = −0.07614 log ν − 1.80531, R^2 = 0.994), confirming the irreversibility of the reduction process, which suggests the presence of chemically coupled reactions during the electrochemical reduction process.[57]

The transfer coefficient (α) was calculated to understand the mechanism of the reduction of PFOA. This parameter reveals the symmetry of the energy barrier during the electron-transfer process, which describes whether the transition state is more similar to the products or the initial reagents.[32] The parameter α is often used to distinguish between the two mechanisms in the reduction of alkyl and aryl halides. According to the following criteria, a value of $\alpha > 0.5$ indicates a stepwise mechanism, whereas a value of $\alpha \ll 0.5$ (usually ≈0.3) implies a concerted mechanism.[28] Therefore, since the Ep_c varies linearly with ν, with a slope $\partial E_p/\partial \log \nu$, α was calculated using eq 4. Likewise, analyzing the difference between the Ep_c and half-peak potential ($E_{p/2}$: potential corresponding at the half-peak current, $i_{p/2}$),[27] α was alternatively calculated with eq 5

$$\frac{\partial E_p}{\partial \log \nu} = -\frac{1.15RT}{\alpha F} \tag{4}$$

$$E_p - E_{p/2} = \frac{1.857RT}{\alpha F} \tag{5}$$

Table 1 shows the α values obtained for the reduction of PFOA performed on a gold surface. In both calculations, the transfer coefficient is around 0.38, indicating a concerted mechanism. Stepwise mechanisms typically occur when low-lying empty orbitals are available to host the incoming electron transiently. In this PFOA case, no aromatic rings are present, so the dissociation of the C−F bond is purely concerted, similar to what is observed for aliphatic halides.[58]

Table 1. Voltammetric Data for the Reduction of 1 mM PFOA + 0.5 M $KHCO_3$ (pH 9.5) Obtained Using a Gold Electrode

parameter	value
$-\partial E_p/\partial \log \nu$	76.1 mV dec^{-1}
$\lvert E_p - E_{p/2}\rvert^a$	119.6 mV
$E^{0\prime}$	−1.805 V
α^b	0.38
α^c	0.39

[a]Average of the values obtained at ν = 50 − 200 mV s^{-1}. [b]Obtained from eq 4. [c]Obtained from eq 5.

Figure S7d shows the plot of the peak reduction potential Ep_c versus the log of the scan rate. The y-intercept corresponds to a formal potential ($E^{0\prime}$) of −1.80 V vs Ag/AgCl. The thermodynamic implication of this "low" value, considering the high energy needed to dissociate the C−F bond, is related to the surface and reorganization effects of PFOA during the dissociative electron transfer (DET). As mentioned earlier, the Langmuir isotherms provide evidence of the strong adsorption of PFOA onto the Au surface. This strong adsorption is reflected in improving the kinetics of the charge transfer as the C−F bond is being weakened due to the F···Au and R···Au interactions decreasing the activation energy of the DET in the outer-sphere pathway. Once the C−F is dissociated, F^- adsorption to the Au surface is thermodynamically favorable due to the high affinity of F^- to Au (ΔE = −134.9 kJ mol^{-1}).[59] These coupled Au adsorption processes support the "low" observed formal PFOA reduction potential.[30] The lowering of the overpotential of the reduction potential in noble metal surfaces has been reported in the literature in the reduction of aryl bromides,[30] benzyl halides,[60] and other organic halides[61] by evaluating the peak potential differences between a noncatalytic electrode, such as a glassy carbon electrode (GCE), and the catalytic active electrodes, in terms of $Ep_M - Ep_{GCE}$.[62] Gold electrodes have shown an overpotential lowering of around 0.1−0.8 V for bromothiophenes and bromobenzenes[63] and other organic halides.[62]

The electron-transfer event was analyzed using the approach described by Marcus−Hush to provide a more fundamental explanation of the reduction of PFOA. While this model does not apply to outer-sphere electron-transfer processes (since the harmonic approximation for the reorganization energy is not compatible with bond breaking), it can be adapted for a heterogeneous charge transfer[64] since the first electron transfer is the rate-limiting step (which occurs in our case). The theory predicts that the free energy in the transition state ($\Delta G^{\ddagger}$) is a quadratic function of the standard free energy of reaction ΔG^0, as shown in eq 6

$$\Delta G^{\ddagger} = \Delta G_0^{\ddagger}\left(1 + \frac{\Delta G^{\circ}}{4\Delta G_0^{\ddagger}}\right)^2 \tag{6}$$

Since $\Delta G^0 = -nF(E - E^0)$, it is possible to calculate, for an electrode reaction, the free energy in the transition state from the standard potential (E^0) at any electrode potential (E), as shown in eq 7.

$$\Delta G^{\ddagger} = \Delta G_0^{\ddagger}\left(1 + \frac{F(E - E^0)}{4\Delta G_0^{\ddagger}}\right)^2 \tag{7}$$

where E and E^0 are expressed in volts (V) and the free energies in eV.[65] To calculate $\Delta G^{\ddagger}$, it is necessary to introduce the energy required to dissociate the C−X bond, represented as the bond dissociation energy (D_b). Using computational methods, we calculated a D_b of 447.76 kJ mol^{-1} for the PFOA C−F bond, which was used throughout these calculations. The standard free energy in the transition state ($\Delta G_0^{\ddagger}$) can be calculated using eq 8

$$\Delta G_0^{\ddagger} = \frac{D_b + \lambda_0}{4} \tag{8}$$

The effect of the solvent during the transition state is considered in terms of its reorganization energy (λ_0).[66] The energy required for the solvent molecules to be in the ideal position to disperse the charge-transfer state without charge transfer having occurred can be calculated according to Marcus's theory,[67] as in eq 9

https://doi.org/10.1021/jacs.4c00443
J. Am. Chem. Soc. 2024, 146, 10687−10698

Table 2. Determination of the C−F Bond Dissociation Energies Using the Marcus-Hush model for the PFOA Electron-Transfer Reaction in 0.5 M $KHCO_3$ at pH 9.5

scan rate (mV s^{-1})	$\frac{a_{F-}\ (Å)}{a_{PFOA}\ (Å)}$ a (Å)	λ_0 (eV)	k_s (cm s^{-1})	$\Delta G_0^{\ddagger}$ (eV)	DC−F (eV)	$\Delta G^{\ddagger}$ (eV)	α_{exp}	α_{pred}
50	1.36 6.59 2.44	0.9	0.0341	1.385	4.64	2.429	0.38	0.27

$$\lambda_0 = \left(\frac{1}{D_{op}} - \frac{1}{D_s}\right)\frac{e_0^2}{4a} \tag{9}$$

and with a Hush-like estimation using eq 10

$$\lambda_0 = \left(\frac{1}{D_{op}} - \frac{1}{D_s}\right)\frac{e_0^2}{2a} \tag{10}$$

D_{op} and D_s are the optic and static dielectric constants of the solvent, with values for water of 1.78 and 80.4 F m^{-1}, respectively.[68] The sphere equivalent radius is represented by a, and e_0 is the charge of the electron. The Marcus−Hush estimation for λ_0 requires a more realistic value of a to approximate the solvent organization better and to show how it interacts with C−F during the transition state. Therefore, we used previous estimates by the arithmetic measure of the halogen radius (a_X = F^-), and the radius of the sphere correspondent to the whole molecule (a_{RX} = a_{PFOA}), itself derived from the density (ρ) and the molar mass (M).[69]

$$a_{RX} = \sqrt[3]{\frac{3M}{4N_A\rho}} \tag{11}$$

Moreover, a was calculated with eq 12.

$$a = \frac{a_X(2a_{RX} - a_X)}{a_{RX}} \tag{12}$$

Using the theoretical values of $\Delta G_0^{\ddagger}$ and λ_0 (Table 2), we related the reorganization of PFOA during its reduction to the gold surface. From the experimental data obtained of the peak potentials of the irreversible voltammograms, the theory can approximate the activation-free energy at the peak ($\Delta G_p^{\ddagger}$), at a given scan rate.[65] The heterogeneous standard rate constant (k_s) may be obtained from eq 13

$$E_p = \Delta G_p^{\ddagger} = E^{\circ} - 0.78\frac{RT}{\alpha F} + \frac{RT}{\alpha F}\ln\frac{k_s}{\sqrt{\frac{\alpha DFv}{RT}}} \tag{13}$$

The PFOA diffusion coefficient (D) was calculated using the Stokes−Einstein relationship (eq 14)

$$D = \frac{Tk_b}{6\pi r\eta} \tag{14}$$

where k_b is Boltzmann's constant and η is the viscosity of the solution (0.001002 kg m^{-1} s^{-1} for water at 20 °C). The value of a was calculated with eq 12, and it was used as the radius of the spherical particle (r). The calculated D value is 8.77×10^{-6} cm^2 s^{-1}. Equation 15 shows the relationship between $\Delta G_0^{\ddagger}$ and ΔG^0, which has the same quadratic form, as shown in eq 6, allowing us to calculate the theoretical α.[70]

$$\alpha = \frac{\partial\Delta G^{\ddagger}}{\partial\Delta G^{\circ}} = \frac{1}{2}\left(1 + \frac{\Delta G^{\circ}}{4\Delta G_0^{\ddagger}}\right) \tag{15}$$

Equation 15 yields a calculated value of α_{pred} of 0.27, which is in close agreement with the measured Butler−Volmer value (α_{exp}) of 0.38. Both values of α are consistent with a concerted DET mechanism. All of the parameters previously described are summarized in Table 2. The solvent reorganization parameter λ_0 is 0.9 eV, which suggests that it is challenging for water to be around the C and F atoms before DET. This is consistent with the hydrophobic nature of the perfluorinated chain. The inefficient interactions between PFOA and water imply that the C−F bond is not in the best geometry to be broken during DET. In addition, the small size of the fluorine atoms, which requires water molecules to surround it, contributes to increasing the reorganization energy.[66] The larger value of $\Delta G^{\ddagger}$ with respect to λ_0 suggests that it is the dominant factor in the activation barrier. The values for $\Delta G_0^{\ddagger}$ and $\Delta G^{\ddagger}$ are higher than the reported values for other alkyl and aryl halides,[58,66,71] which is consistent with the high dissociation energy of the C−F bond.

A potential diagram of the reaction is shown in Figure 3. The potential energy profiles are strongly associated with the capacity of each species to be absorbed into the Au surface

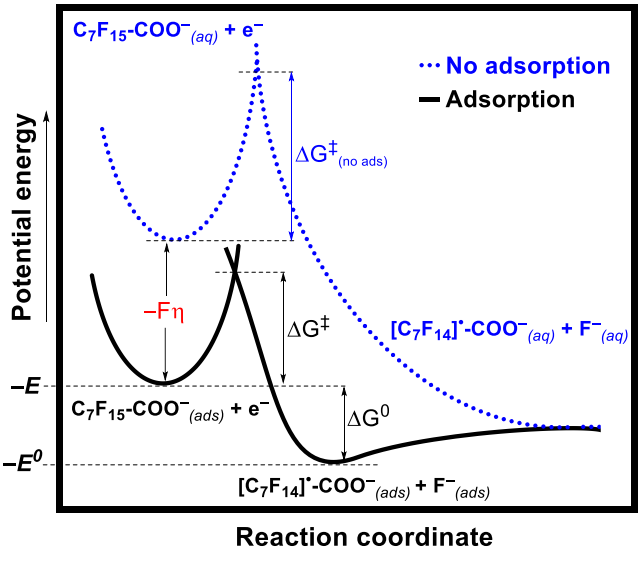

Figure 3. Potential energy diagram for a dissociative electron transfer to PFOA at a gold electrode based on eqs 6−10. Comparison of the energy profile in the absence (dotted blue line) and presence (black line) of adsorption during the reduction event. The $\Delta G_{(no\ ads)}^{\ddagger}$ represents the free energy of the transition state in the absence of adsorption. The overpotential ($\eta = E^{\circ} - E$) indicates the difference between the applied potential in the absence and presence of the adsorption and is shown in terms of energy as $-F\eta$.

https://doi.org/10.1021/jacs.4c00443
J. Am. Chem. Soc. 2024, 146, 10687−10698

during the electron transfer. The dotted blue line shows the DET in a hypothetical case where the PFOA is not adsorbed. The reduction reaction in the absence of adsorption requires a $\Delta G^{\ddagger}$ larger than that when the PFOA substrate is adsorbed to the gold surface. Therefore, an overpotential is required ($\eta = E^{\circ} - E$), which can be expressed in terms of energy as $-F\eta$. In our case, the strong adsorption of PFOA into the gold surface lowers the energy profiles. Upon adsorption, an electron is transferred to produce $[C_7F_{14}-COO^-]_{(ads)}^{\bullet}$ and $F_{(ads)}^-$ species, which also interact strongly with the gold surface, lowering $\Delta G^{\ddagger}$ and decreasing the overpotential.

Bulk electrolysis of 1 mM PFOA at a constant potential was performed to obtain more information about the electrochemical reduction. As shown in Figure 4a, most of the charge

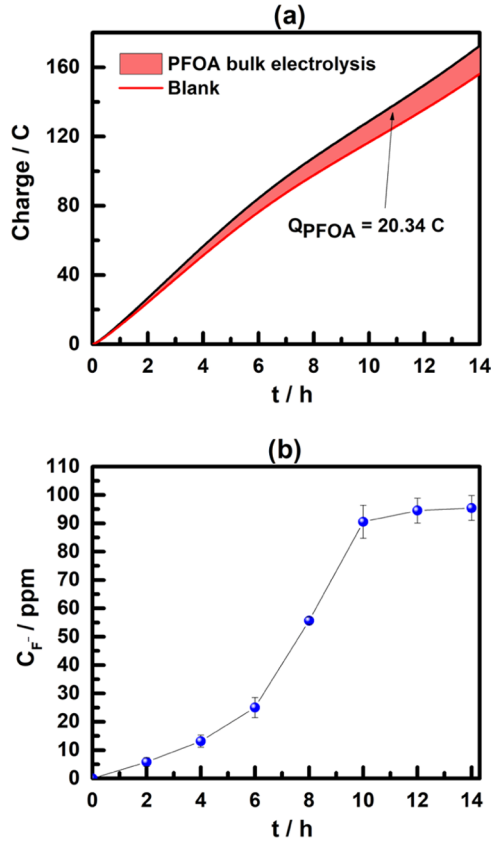

Figure 4. Controlled-potential electrolysis of 1 mM PFOA + 0.5 M $KHCO_3$ (pH 9.5). (a) Charge vs time plot. (b) Variation of the F^- ions concentration vs time plot. E_{app} = −1.80 V vs Ag/AgCl.

passed during the bulk electrolysis is consumed for the water reduction. The resulting charge spent during the PFOA reduction is Q_{exp} = 20.34 C. Considering that 4.82 C (Q_{theo} = 2 F n_{PFOA}) is required to remove one fluorine atom, we expect a PFOA chain with at least four hydrogen atoms. The F^- ions concentration was recorded during the electrolysis to confirm the defluorination process. Figure 4b shows the C_{F^-} increase during 14 h, and the stoichiometric number of fluorine atoms exchanged was calculated with eq 16.

$$n_F = \frac{C_{F^-}}{C_{PFOA}}\left(\frac{MW_{PFOA}}{MW_F}\right) \quad (16)$$

Increasing the bulk electrolysis time did not show a significant increase in the concentration of F^- ions after 14 h. A total of 6 fluoride atoms were determined, suggesting that the defluorination process is ineffective when carried out into a gold electrode, as there are major kinetic and thermodynamic limitations, showing how difficult it is to hydrogenate the PFOA chain completely.

The PFOA solution and the bulk electrolysis products were analyzed by ^{19}F NMR spectroscopy. As shown in Figure 5a (blue line), the spectrum shows the typical signals of PFOA (i.e., $-CF_3$ at −80.16 ppm and secondary carbons (F_2-F_7) in the range from −121 to −127 ppm).[72] Figure 5a (black line) shows a close-up of the $F_2 - F_7$ region. After bulk electrolysis (blue line), the intensity of some signals decreases. Integration of the signals for F_4, F_5, and F_7 reveals a total integral of 1, which suggests that the defluorination process was most likely carried out on these carbons. The apparent release of 3 fluorine atoms suggests a trihydrogenated PFOA chain or the formation of 3 monohydrogenated chains. The ^1H NMR spectrum (Figure 5b) shows a new signal at 5.1 ppm, which suggests the formation of a new hydrogenated compound, supporting our previous description.

We previously observed that six fluorine atoms leave the PFOA, suggesting that some fluorine atoms may leave the chain in a nonelectrochemical way and thus generate byproducts other than hydrogenated chains. UV−vis spectra (Figure S8) of the working solution after 14 h of bulk electrolysis show a well-defined band at λ_{max} of 292 nm, which suggests the formation of an unsaturated chain ($[C_7F_{13}-COO]^-$) resulting from a bimolecular elimination (E2) reaction.[32] This is further supported by ESI(−) mass spectrometry (Figure S9). Before electrolysis, a mass corresponding to PFOA is observed at a m/z of 412.88 with its respective fragmentations. After bulk electrolysis, a m/z of 394.96 m/z is observed. This mass is attributed to the monohydrogenated species $[C_7F_{14}H-COO]^-$ which has previously been reported as a reduction product.[73] In addition, a m/z of 374.97 corresponding to the monounsaturated chain $[C_7F_{13}-COO]^-$ is observed. No m/z values corresponding to polyhydrogenated chains were identified. We did not find evidence for the formation of polyunsaturated alkene species. The required conditions to perform E2-type elimination are consistent with our system because the OH^- ions are electrogenerated *in situ* as byproducts of the reduction of PFOA. The OH^- ions can remove the inserted hydrogen to produce an alkene and promote the release of an F^- ion.[74] Therefore, we propose a mechanism that requires a two-electron reduction that yields $[C_7F_{14}H-COO]^-$ and leads to the subsequent transformation to $[C_7F_{13}-COO]^-$ through a bimolecular elimination (E2) reaction.

Through a DET mechanism, it is possible to produce partially hydrogenated chains due to H/F exchange. Figure 5c shows a proposed mechanism. Initially, PFOA is strongly adsorbed into the inner Helmholtz plane (IHP) since this is the reaction site for specifically adsorbed species. An electron transfer generates the radical species $[C_7F_{14}-COO^-]^{\bullet}$, which promotes the release of F^- ions from the secondary carbons. A second electron transfer generates carbanion species $[C_7F_{14}-COO^-]^-$, which is likely not adsorbed and can move to the outer Helmholtz plane (OHP) by the negatively charged electrode. The electrogenerated carbanion can quickly take a proton from the adsorbed water to yield a $[C_7F_{14}H-COO]^-$ anion. The reaction is completed when the F^- ions desorb and

https://doi.org/10.1021/jacs.4c00443
J. Am. Chem. Soc. 2024, 146, 10687−10698

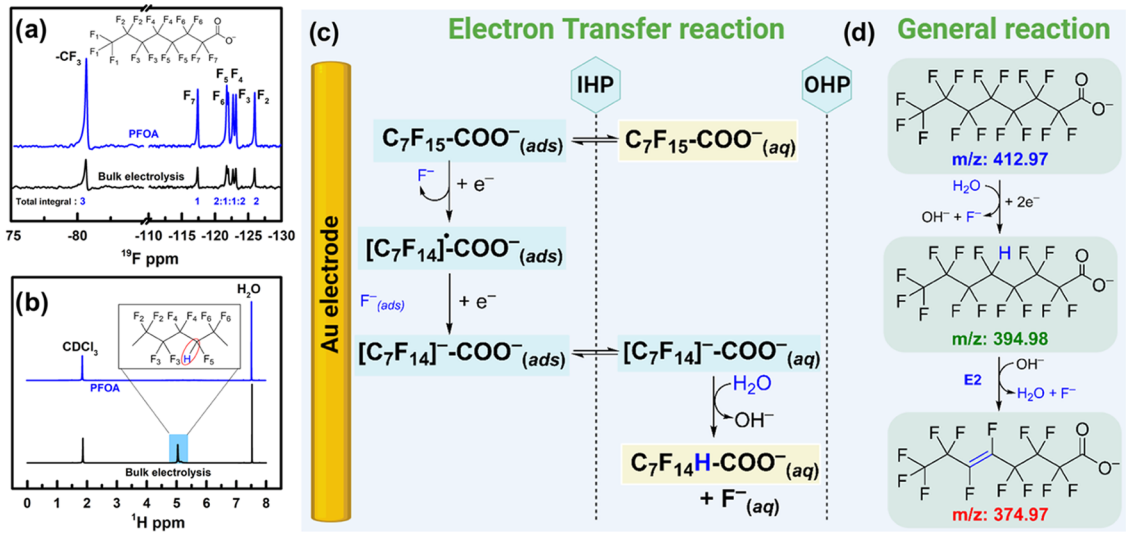

Figure 5. (a) ^{19}F NMR spectra before and after bulk electrolysis of 1 Mm PFOA + 0.5 M $KHCO_3$ (pH 9.5). (b) ^{1}H NMR spectra before and after bulk electrolysis. (c) Proposed mechanism to explain the reduction of PFOA. (d) General reactions involved in the reduction reaction.

diffuse into the bulk solution, regenerating the surface-active sites of the electrode. The general reaction is presented in Figure 5d, as well as the proposed formation of alkenes via an E2-type reaction.

We turned to density functional theory (DFT) calculations at the TPSSh-D3/def2-TZVP level of theory with the SMD solvation model to explore the electrochemical reduction of PFOA and its selectivity along the fluorinated chain. Table S2 summarizes the resulting energies for all species involved in the electroreduction of PFOA. The reduction potentials of the different redox steps (i.e., eqs 18−19) of the concerted mechanism (eqs 17−20) were calculated:

$$C_7F_{15}COOH \rightleftarrows [C_7F_{15}COO]^- + H^+ \quad (17)$$

$$[C_7F_{15}COO]^- + e^- \rightarrow [C_7F_{14}COO]^{\bullet -} + F^- \quad (18)$$

$$[C_7F_{14}COO]^{\bullet -} + e^- \rightarrow [C_7F_{14}COO]^{2-} \quad (19)$$

$$[C_7F_{14}COO]^{2-} + H_2O \rightarrow [C_7F_{14}HCOO]^- + OH^- \quad (20)$$

We also calculated the reduction potential of the first electron transfer of a stepwise mechanism, which includes the formation of $[C_7F_{14}COO]^{\bullet 2-}$ species, as shown in eq 21.

$$[C_7F_{15}COO]^- + e^- \rightarrow [C_7F_{15}COO]^{\bullet 2-} \quad (21)$$

The experimental $E^{0\prime}$ for the electroreduction of PFOA was estimated to be −1.80 V vs Ag/AgCl, and the calculated standard potential for eq 21 is −3.03 vs Ag/AgCl (Table 3). The difference potential is 1.23 V, which is less negative than the computationally calculated reduction potential for the stepwise reaction. The latter suggests that forming the radical anion $[C_7F_{15}COO]^{\bullet 2-}$ is more thermodynamically intricate than the immediate splitting of the C−F bond upon reduction in a concerted fashion. The calculated reduction potentials for eq 18 range from −2.06 to −2.52 V vs Ag/AgCl, depending upon the position of the C−F bond being dissociated (C_n). These results are consistent with our experimentally observed reduction potentials and support a concerted mechanism for the reductive PFOA C−F dissociation. Other reports have

Table 3. Calculated Reduction Potentials (E^0) in Water for the Reductive Defluorination of PFOA at C_2−C_8

redox process	E^0 (V) vs SHE	E^0 (V) vs Ag/AgCl
reaction A[a]	−2.84	−3.03
reaction B[b]		
C_2[d]	−1.87	−2.06
C_3	−1.91	−2.11
C_4	−1.85	−2.05
C_5	−1.85	−2.05
C_6	−1.84	−2.04
C_7	−1.97	−2.16
C_8	−2.33	−2.53
reaction C[c]		
C_2[d]	−0.80	−0.99
C_3	−0.46	−0.66
C_4	−0.38	−0.58
C_5	−0.14	−0.33
C_6	−0.07	−0.26
C_7	−0.01	−0.21
C_8	−0.43	−0.63

[a]Reaction A: $[C_7F_{15}COO]^- + e^- \rightarrow [C_7F_{15}COO]^{\bullet 2-}$. [b]Reaction B: $[C_7F_{15}COO]^- + e^- \rightarrow [C_7F_{14}COO]^{\bullet -} + F^-$. [c]Reaction C: $[C_7F_{14}COO]^{\bullet -} + e^- \rightarrow [C_7F_{14}COO]^{2-}$. [d]$C_2$ corresponds to the vicinal C atom of the COOH group. Calculations were performed at the TPSSh-D3/def2-TZVP level of theory and the SMD solvation model.

obtained reduction potentials in the range of −2.50 to −2.95 V vs SHE.[73]

Although the formation of a $[C_7F_{15}COO]^{\bullet 2-}$ radical may occur at an appropriate potential (see Figure 6), the computed energy barriers, represented by the Gibbs free energy difference between the $[C_7F_{15}COO]^{\bullet 2-}$ intermediate and the transition state (TS), lie between 1.06 and 5.58 kcal mol^{-1} depending on the dissociation site (Table S3). The low energy barriers predicted indicate a transition state of minimal energy, suggesting that, if formed, the $[C_7F_{15}COO]^{\bullet 2-}$ intermediate is short-lived and will quickly transform into $[C_7F_{14}COO]^{\bullet -}$ + F^- species, also in agreement with a concerted-like mechanism. The subsequent reduction described in eq 19 is calculated to be in the range of −0.21 to −0.99 V vs Ag/AgCl. This range is

https://doi.org/10.1021/jacs.4c00443
J. Am. Chem. Soc. 2024, 146, 10687−10698

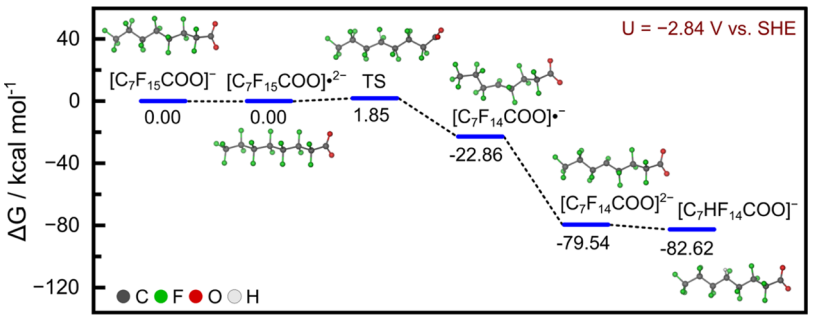

Figure 6. Calculated Gibbs free energy potential energy surface for the electroreduction of PFOA at U = −2.84 V vs SHE. The reaction is shown for the C_4 dissociation site as an illustration. Note that although the reaction is modeled for a stepwise mechanism, the small energy barrier for the TS shows the instantaneous formation of $[C_7F_{14}COO]^{\bullet-}$ + F^- (i.e., the radical anion $[C_7F_{15}COO]^{\bullet 2-}$ is short-lived), which supports a concerted mechanism for PFOA electroreduction. Calculations were performed at the TPSSh-D3/def2-TZVP/SMD level of theory.

more positive than those potentials calculated for eq 18 and suggests that they are more thermodynamically favorable. Upon formation, the $[C_7F_{14}{-}COO]^{2-}$ carbanion interacts with a water molecule, forming a $[C_7HF_{14}COO]^-$ anion (ΔG = −3.1 kcal mol^{-1}) as expected for the reduction of alkyl halides. The predicted thermodynamics for each dissociation site (C_n center) where the C−F dissociation may occur is provided in Table 3 and Figure S10. The computed results show little thermodynamic preference among C_2 − C_7 for the C−F dissociation event. The calculated reduction potentials for the redox events for these sites (described in eq 18) are in the range of −2.06 to −2.16 V Ag/AgCl, which is very close to the expected computational error. Because there is little preference among the C_2 − C_7, a mixture of species at the end of the electrocatalytic process is expected. The above is consistent with the ^{19}F − ^1H NMR data because it shows that at least three monohydrogenated carbon chains are present after 14 h of bulk electrolysis. Figure 7 shows the HOMO and LUMO of the PFOA molecule calculated in water. The HOMO is centered on the carboxylic group, while the LUMO is composed of the antibonding interaction between the *p* orbitals of the carbon chain and the *s* orbitals of the fluorine atoms. Occupying the LUMO upon reduction destabilizes these C−F bonds, leading to their dissociation. The electron density difference map ($\Delta\rho$) between $[C_7F_{15}COO]^-$ and $[C_7F_{15}COO]^{\bullet 2-}$ shows that the incoming electron accumulates ($\Delta\rho > 0$, red lobes) at the C and F atoms along the fluorinated chain in agreement with our experimental observations.

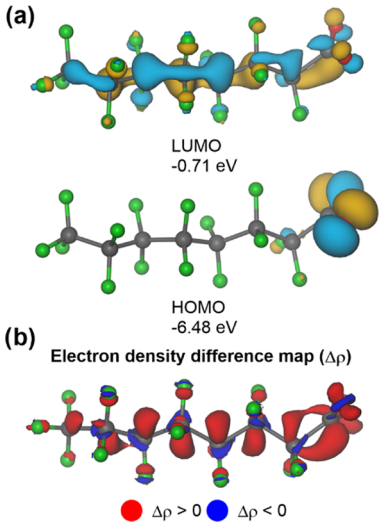

Figure 7. (a) HOMO and LUMO orbitals of PFOA anion plotted at an isovalue of ±0.06. (b) Electron density difference map ($\Delta\rho$ = ±0.004 a.u.) of the one-electron reduction of PFOA anion calculated at the TPSSh-D3/def2-TZVP level of theory.

CONCLUSIONS

The reduction of PFOA was performed in alkaline media on a gold electrode and corresponds to an electrochemical two-electron process with chemically coupled reactions, resulting in a defluorination event. The C−F bond energy is the main barrier to performing PFOA degradation. However, the gold surface decreases the PFOA reduction overpotential due to the strong surface adsorption of PFOA. Linear sweep voltammetry shows a linear relationship between the peak current and the scan rate, suggesting a mass transport controlled by adsorption. The Langmuir isotherm model shows a K_A of 10^7 cm^3 mol^{-1} under negative potential conditions, which confirms the preference of gold surface to adsorb PFOA. These PFOA−Au interactions play an important role in weakening the C−F bond and enhancing the electron-transfer kinetics by decreasing the overpotential.

The electron-transfer coefficient (α) calculated for the reduction of PFOA is lower than 0.5, which suggests C−F dissociation by an electrochemical concerted mechanism. Using a Marcus−Hush theory model, we calculated the solvent reorganization energy (λ_0 = 0.9 eV), which reveals a large electrostatic repulsion between the perfluorinated chain and water as expected from the surfactant properties of PFOA. Moreover, the calculated free energy of the transition state ($\Delta G‡$ = 2.43 eV) put forward that thermodynamics is still the limiting barrier of the reaction, even with the electrocatalytic properties of the gold electrode. The H/F exchange in the PFOA chain was confirmed by ^{19}F − ^1H NMR studies, which show a mixture of partially hydrogenated compounds. Quantification of F^- ions shows that at least three fluorine atoms can be displaced by hydrogen and that unsaturated chains can be formed as a byproduct. This shows that the defluorination process can be accomplished, even with strong competition against the water reduction reaction. Density functional theory (DFT) calculations also support the concerted mechanism for the reductive defluorination of PFOA. The calculated reduction potentials for the first redox event of the concerted PFOA C−F dissociation are in the range of −2.06 to −2.52 V vs Ag/AgCl depending on the position of the C−F bond being dissociated, which is in close agreement with the experimental estimated $E^{0\prime}$ value for the

https://doi.org/10.1021/jacs.4c00443
J. Am. Chem. Soc. 2024, 146, 10687−10698

electroreduction of PFOA of −1.80 V vs Ag/AgCl. Minor thermodynamic differences were observed for the C−F bond dissociation along C_2 − C_7 sites, implying the formation of a mixture of species at the end of the bulk electrolysis, in agreement with our experimental values.

■ ASSOCIATED CONTENT

Supporting Information

The Supporting Information is available free of charge at https://pubs.acs.org/doi/10.1021/jacs.4c00443.

> Electrochemical characterization, pH effect on the reduction of PFOA, adsorption isotherms, C_{dl} measurements, ECSA and K_A calculations, scan rate diagnosis, UV−vis spectra and mass spectrometry of the degradation products, and DFT energies and Cartesian coordinates of the resultant optimized geometries for all calculations (PDF)

■ AUTHOR INFORMATION

Corresponding Author

Dino Villagrán − *Department of Chemistry and Biochemistry, The University of Texas at El Paso, El Paso, Texas 79968, United States; Nanosystems Engineering Research Center for Nanotechnology-Enabled Water Treatment (NEWT), El Paso, Texas 79968, United States;* orcid.org/0000-0002-5798-3584; Email: dino@utep.edu

Authors

Jonathan J. Calvillo Solís − *Department of Chemistry and Biochemistry, The University of Texas at El Paso, El Paso, Texas 79968, United States; Nanosystems Engineering Research Center for Nanotechnology-Enabled Water Treatment (NEWT), El Paso, Texas 79968, United States;* orcid.org/0000-0003-2928-488X

Christian Sandoval-Pauker − *Department of Chemistry and Biochemistry, The University of Texas at El Paso, El Paso, Texas 79968, United States; Nanosystems Engineering Research Center for Nanotechnology-Enabled Water Treatment (NEWT), El Paso, Texas 79968, United States;* orcid.org/0000-0002-7831-331X

David Bai − *Department of Chemistry and Biochemistry, The University of Texas at El Paso, El Paso, Texas 79968, United States; Nanosystems Engineering Research Center for Nanotechnology-Enabled Water Treatment (NEWT), El Paso, Texas 79968, United States*

Sheng Yin − *Department of Chemistry and Biochemistry, The University of Texas at El Paso, El Paso, Texas 79968, United States; Nanosystems Engineering Research Center for Nanotechnology-Enabled Water Treatment (NEWT), El Paso, Texas 79968, United States*

Thomas P. Senftle − *Department of Chemical and Biomolecular Engineering, Rice University, Houston, Texas 770052, United States; Nanosystems Engineering Research Center for Nanotechnology-Enabled Water Treatment (NEWT), El Paso, Texas 79968, United States;* orcid.org/0000-0002-5889-5009

Complete contact information is available at: https://pubs.acs.org/10.1021/jacs.4c00443

Author Contributions

The manuscript was written through the contributions of all authors. All authors have approved the final version of the manuscript.

Notes

The authors declare no competing financial interest.

■ ACKNOWLEDGMENTS

This work was partially funded by the Welch Foundation AH-2083-20210327 and the NSF Nanosystems Engineering Research Center for Nanotechnology-Enabled Water Treatment (NEWT) (ERC-1449500, USA). The authors thank UTEP HPC JAKAR Cluster for the computational resources provided free of charge. C.S.-P. thanks the Texas Higher Education Coordinating Board for his Good Neighbor Scholarship.

■ ABBREVIATIONS

PFOA:perfluorooctanoic acid
DET:dissociative electron transfer
LSV:linear sweep voltammetry

■ REFERENCES

(1) Lamichhane, H. B.; Arrigan, D. W. M. Electroanalytical Chemistry of Per- and Polyfluoroalkyl Substances. *Curr. Opin. Electrochem.* **2023**, *40*, No. 101309.

(2) Leung, S. C. E.; Shukla, P.; Chen, D.; Eftekhari, E.; An, H.; Zare, F.; Ghasemi, N.; Zhang, D.; Nguyen, N.-T.; Li, Q. Emerging Technologies for PFOS/PFOA Degradation and Removal: A Review. *Sci. Total Environ.* **2022**, *827*, No. 153669.

(3) Sharma, S.; Shetti, N. P.; Basu, S.; Nadagouda, M. N.; Aminabhavi, T. M. Remediation of Per- and Polyfluoroalkyls (PFAS) via Electrochemical Methods. *Chem. Eng. J.* **2022**, *430*, No. 132895.

(4) Javed, H.; Lyu, C.; Sun, R.; Zhang, D.; Alvarez, P. J. J. Discerning the Inefficacy of Hydroxyl Radicals during Perfluorooctanoic Acid Degradation. *Chemosphere* **2020**, *247*, No. 125883.

(5) Yin, S.; Villagrán, D. Design of Nanomaterials for the Removal of Per- and Poly-Fluoroalkyl Substances (PFAS) in Water: Strategies, Mechanisms, Challenges, and Opportunities. *Sci. Total Environ.* **2022**, *831*, No. 154939.

(6) Veciana, M.; Bräunig, J.; Farhat, A.; Pype, M.-L.; Freguia, S.; Carvalho, G.; Keller, J.; Ledezma, P. Electrochemical Oxidation Processes for PFAS Removal from Contaminated Water and Wastewater: Fundamentals, Gaps and Opportunities towards Practical Implementation. *J. Hazard. Mater.* **2022**, *434*, No. 128886.

(7) Mirabediny, M.; Sun, J.; Yu, T. T.; Åkermark, B.; Das, B.; Kumar, N. Effective PFAS Degradation by Electrochemical Oxidation Methods-Recent Progress and Requirement. *Chemosphere* **2023**, *321*, No. 138109.

(8) Xie, J.; Zhang, C.; David Waite, T. Integrated Flow Anodic Oxidation and Ultrafiltration System for Continuous Defluorination of Perfluorooctanoic Acid (PFOA). *Water Res.* **2022**, *216*, No. 118319.

(9) Zhang, Z.; Sarkar, D.; Datta, R.; Deng, Y. Adsorption of Perfluorooctanoic Acid (PFOA) and Perfluorooctanesulfonic Acid (PFOS) by Aluminum-Based Drinking Water Treatment Residuals. *J. Hazard. Mater. Lett.* **2021**, *2*, No. 100034.

(10) Steenland, K.; Fletcher, T.; Stein, C. R.; Bartell, S. M.; Darrow, L.; Lopez-Espinosa, M.-J.; Barry Ryan, P.; Savitz, D. A. Review: Evolution of Evidence on PFOA and Health Following the Assessments of the C8 Science Panel. *Environ. Int.* **2020**, *145*, No. 106125.

(11) Liang, L.; Pan, Y.; Bin, L.; Liu, Y.; Huang, W.; Li, R.; Lai, K. P. Immunotoxicity Mechanisms of Perfluorinated Compounds PFOA and PFOS. *Chemosphere* **2022**, *291*, No. 132892.

(12) Jane L Espartero, L.; Yamada, M.; Ford, J.; Owens, G.; Prow, T.; Juhasz, A. Health-Related Toxicity of Emerging per- and Polyfluoroalkyl Substances: Comparison to Legacy PFOS and PFOA. *Environ. Res.* **2022**, *212*, No. 113431.
(13) Wee, S. Y.; Aris, A. Z. Revisiting the "Forever Chemicals", PFOA and PFOS Exposure in Drinking Water. *npj Clean Water* **2023**, *6* (1), No. 57.
(14) Karatas, O.; Kobya, M.; Khataee, A.; Yoon, Y. Perfluorooctanoic Acid (PFOA) Removal from Real Landfill Leachate Wastewater and Simulated Soil Leachate by Electrochemical Oxidation Process. *Environ. Technol. Innovation* **2022**, *28*, No. 102954.
(15) Liu, Y.; Fan, X.; Quan, X.; Fan, Y.; Chen, S.; Zhao, X. Enhanced Perfluorooctanoic Acid Degradation by Electrochemical Activation of Sulfate Solution on B/N Codoped Diamond. *Environ. Sci. Technol.* **2019**, *53* (9), 5195−5201.
(16) Galicia, M.; González-Fuentes, M. A.; Valencia, D. P.; González, F. J. The Effect of Substituents on the Anodic Oxidation of Aliphatic Carboxylates and the Passage towards a Pseudo-Kolbe Reaction. *J. Electroanal. Chem.* **2012**, *672*, 28−33.
(17) Chen, Z.; Wang, X.; Feng, H.; Chen, S.; Niu, J.; Di, G.; Kujawski, D.; Crittenden, J. C. Electrochemical Advanced Oxidation of Perfluorooctanoic Acid: Mechanisms and Process Optimization with Kinetic Modeling. *Environ. Sci. Technol.* **2022**, *56* (20), 14409−14417.
(18) Song, D.; Qiao, B.; Wang, X.; Zhao, L.; Li, X.; Zhang, P.; Yao, Y.; Chen, H.; Zhu, L.; Sun, H. Degradation of Perfluorooctanoic Acid by Chlorine Radical Triggered Electrochemical Oxidation System. *Environ. Sci. Technol.* **2023**, *57* (25), 9416−9425.
(19) Hou, J.; Li, G.; Liu, M.; Chen, L.; Yao, Y.; Fallgren, P. H.; Jin, S. Electrochemical Destruction and Mobilization of Perfluorooctanoic Acid (PFOA) and Perfluorooctane Sulfonate (PFOS) in Saturated Soil. *Chemosphere* **2022**, *287*, No. 132205.
(20) Marks, R. G. H.; Kerpen, K.; Diesing, D.; Telgheder, U. Electrochemical Degradation of Perfluorooctanoic Acid in Aqueous Solution by Boron-Doped Diamond Electrodes under Pulsed Voltage Conditions. *J. Electroanal. Chem.* **2021**, *895*, No. 115415.
(21) Wang, C.; Zhang, T.; Yin, L.; Ni, C.; Ni, J.; Hou, L.-A. Enhanced Perfluorooctane Acid Mineralization by Electrochemical Oxidation Using Ti3+ Self-Doping TiO2 Nanotube Arrays Anode. *Chemosphere* **2022**, *286*, No. 131804.
(22) Sun, S.; Sun, B.; Wang, Q.; Zhu, X.; Liu, H.; Liu, J. Efficient Defluorination of PFOA by Microwave Discharge Plasma in Liquid: Influence of Actual Water Environment Factors. *J. Water Process Eng.* **2023**, *55*, No. 104091.
(23) Long, M.; Donoso, J.; Bhati, M.; Elias, W. C.; Heck, K. N.; Luo, Y.-H.; Lai, Y. S.; Gu, H.; Senftle, T. P.; Zhou, C.; Wong, M. S.; Rittmann, B. E. Adsorption and Reductive Defluorination of Perfluorooctanoic Acid over Palladium Nanoparticles. *Environ. Sci. Technol.* **2021**, *55* (21), 14836−14843.
(24) Román Santiago, A.; Baldaguez Medina, P.; Su, X. Electrochemical Remediation of Perfluoroalkyl Substances from Water. *Electrochim. Acta* **2022**, *403*, No. 139635.
(25) Chen, C.; Ma, Q.; Liu, F.; Gao, J.; Li, X.; Sun, S.; Yao, H.; Liu, C.; Young, J.; Zhang, W. Photocatalytically Reductive Defluorination of Perfluorooctanoic Acid (PFOA) Using Pt/La2Ti2O7 Nanoplates: Experimental and DFT Assessment. *J. Hazard. Mater.* **2021**, *419*, No. 126452.
(26) Xiong, X.; Shang, Y.; Bai, L.; Luo, S.; Seviour, T. W.; Guo, Z.; Ottosen, L. D. M.; Wei, Z. Complete Defluorination of Perfluorooctanoic Acid (PFOA) by Ultrasonic Pyrolysis towards Zero Fluoro-Pollution. *Water Res.* **2023**, *235*, No. 119829.
(27) Lou, Y.-Y.; Fontmorin, J.-M.; Amrane, A.; Fourcade, F.; Geneste, F. Metallic Nanoparticles for Electrocatalytic Reduction of Halogenated Organic Compounds: A Review. *Electrochim. Acta* **2021**, *377*, No. 138039.
(28) Isse, A. A.; Gottardello, S.; Durante, C.; Gennaro, A. Dissociative Electron Transfer to Organic Chlorides: Electrocatalysis at Metal Cathodes. *Phys. Chem. Chem. Phys.* **2008**, *10* (17), 2409−2416.
(29) Rondinini, S. B.; Mussini, P. R.; Crippa, F.; Sello, G. Electrocatalytic Potentialities of Silver as a Cathode for Organic Halide Reductions. *Electrochem. Commun.* **2000**, *2* (7), 491−496.
(30) Isse, A. A.; Mussini, P. R.; Gennaro, A. New Insights into Electrocatalysis and Dissociative Electron Transfer Mechanisms: The Case of Aromatic Bromides. *J. Phys. Chem. C* **2009**, *113* (33), 14983−14992.
(31) Huang, B.; Sun, Z.; Sun, G. Recent Progress in Cathodic Reduction-Enabled Organic Electrosynthesis: Trends, Challenges, and Opportunities. *eScience* **2022**, *2* (3), 243−277, DOI: 10.1016/j.esci.2022.04.006.
(32) Martin, E. T.; McGuire, C. M.; Mubarak, M. S.; Peters, D. G. Electroreductive Remediation of Halogenated Environmental Pollutants. *Chem. Rev.* **2016**, *116* (24), 15198−15234.
(33) Perini, L.; Durante, C.; Favaro, M.; Agnoli, S.; Granozzi, G.; Gennaro, A. Electrocatalysis at Palladium Nanoparticles: Effect of the Support Nitrogen Doping on the Catalytic Activation of Carbon-halogen Bond. *Appl. Catal., B* **2014**, *144*, 300−307.
(34) Ning, C.; Ma, H.; Pedersen, C. M.; Chang, H.; Wang, Y.; Qiao, Y. Interaction between Environmental Contaminant PFOA and PAMAM in Water: 19F and 1H NMR Studies. *J. Mol. Liq.* **2019**, *283*, 45−50.
(35) Neese, F. The ORCA Program System. *Wiley Interdiscip. Rev.: Comput. Mol. Sci.* **2012**, *2* (1), 73−78.
(36) Tao, J.; Perdew, J. P.; Staroverov, V. N.; Scuseria, G. E. Climbing the Density Functional Ladder: Nonempirical Meta−Generalized Gradient Approximation Designed for Molecules and Solids. *Phys. Rev. Lett.* **2003**, *91* (14), No. 146401.
(37) Staroverov, V. N.; Scuseria, G. E.; Tao, J.; Perdew, J. P. Comparative Assessment of a New Nonempirical Density Functional: Molecules and Hydrogen-Bonded Complexes. *J. Chem. Phys.* **2003**, *119* (23), 12129−12137.
(38) Staroverov, V. N.; Scuseria, G. E.; Tao, J.; Perdew, J. P. Erratum: "Comparative Assessment of a New Nonempirical Density Functional: Molecules and Hydrogen-Bonded Complexes" [J. Chem. Phys. 119, 12129 (2003)]. *J. Chem. Phys.* **2004**, *121* (22), 11507.
(39) Grimme, S.; Antony, J.; Ehrlich, S.; Krieg, H. A Consistent and Accurate Ab Initio Parametrization of Density Functional Dispersion Correction (DFT-D) for the 94 Elements H-Pu. *J. Chem. Phys.* **2010**, *132* (15), No. 154104.
(40) Neese, F.; Wennmohs, F.; Hansen, A.; Becker, U. Efficient, Approximate and Parallel Hartree−Fock and Hybrid DFT Calculations. A 'Chain-of-Spheres' Algorithm for the Hartree−Fock Exchange. *Chem. Phys.* **2009**, *356* (1−3), 98−109.
(41) Marenich, A. V.; Cramer, C. J.; Truhlar, D. G. Universal Solvation Model Based on Solute Electron Density and on a Continuum Model of the Solvent Defined by the Bulk Dielectric Constant and Atomic Surface Tensions. *J. Phys. Chem. B* **2009**, *113* (18), 6378−6396.
(42) Pascual-Ahuir, J. L.; Silla, E. GEPOL: An Improved Description of Molecular Surfaces. I. Building the Spherical Surface Set. *J. Comput. Chem.* **1990**, *11* (9), 1047−1060.
(43) Silla, E.; Tuñón, I.; Pascual-Ahuir, J. L. GEPOL: An Improved Description of Molecular Surfaces II. Computing the Molecular Area and Volume. *J. Comput. Chem.* **1991**, *12* (9), 1077−1088.
(44) Pascual-ahuir, J. L.; Silla, E.; Tuñon, I. GEPOL: An Improved Description of Molecular Surfaces. III. A New Algorithm for the Computation of a Solvent-Excluding Surface. *J. Comput. Chem.* **1994**, *15* (10), 1127−1138.
(45) Trasatti, S. The Absolute Electrode Potential: An Explanatory Note (Recommendations 1986). *Pure Appl. Chem.* **1986**, *58* (7), 955−966.
(46) Lu, T.; Chen, F. Multiwfn: A Multifunctional Wavefunction Analyzer. *J. Comput. Chem.* **2012**, *33* (5), 580−592.
(47) Humphrey, W.; Dalke, A.; Schulten, K. VMD: Visual Molecular Dynamics. *J. Mol. Graphics* **1996**, *14* (1), 33−38.
(48) Nemiwal, M.; Zhang, T. C.; Kumar, D. Graphene-Based Electrocatalysts: Hydrogen Evolution Reactions and Overall Water Splitting. *Int. J. Hydrogen Energy* **2021**, *46* (41), 21401−21418.

(49) Mancinelli, M.; Stevanin, C.; Ardit, M.; Chenet, T.; Pasti, L.; Martucci, A. PFAS as Emerging Pollutants in the Environment: A Challenge with FAU Type and Silver-FAU Exchanged Zeolites for Their Removal from Water. *J. Environ. Chem. Eng.* **2022**, *10* (4), No. 108026.
(50) Galicia, M.; González, F. J. Electrochemical Oxidation of Tetrabutylammonium Salts of Aliphatic Carboxylic Acids in Acetonitrile. *J. Electrochem. Soc.* **2002**, *149* (3), No. D46, DOI: 10.1149/1.1450616.
(51) Burns, D. C.; Ellis, D. A.; Li, H.; McMurdo, C. J.; Webster, E. Experimental pKa Determination for Perfluorooctanoic Acid (PFOA) and the Potential Impact of pKa Concentration Dependence on Laboratory-Measured Partitioning Phenomena and Environmental Modeling. *Environ. Sci. Technol.* **2008**, *42* (24), 9283−9288.
(52) Saeidi, N.; Kopinke, F.-D.; Georgi, A. What Is Specific in Adsorption of Perfluoroalkyl Acids on Carbon Materials? *Chemosphere* **2021**, *273*, No. 128520.
(53) Kazemi, R.; Potts, E. I.; Dick, J. E. Quantifying Interferent Effects on Molecularly Imprinted Polymer Sensors for Per- and Polyfluoroalkyl Substances (PFAS). *Anal. Chem.* **2020**, *92* (15), 10597−10605.
(54) Wang, X.; Ham, S.; Zhang, H.; Wang, Y.; Qiao, R. Adsorption of Model Polyfluoroalkyl Substances on Gold Electrodes for Electroanalytical Applications. *ChemElectroChem* **2023**, *10* (21), No. e202300298.
(55) Gogoi, P.; Yao, Y.; Li, Y. C. Understanding PFOS Adsorption on a Pt Electrode for Electrochemical Sensing Applications. *ChemElectroChem* **2023**, *10* (2), No. e202201006.
(56) Solís, J. C.; Galicia, M. High Performance of MWCNTs - Chitosan Modified Glassy Carbon Electrode for Voltammetric Trace Analysis of Cd(II). *Int. J. Electrochem. Sci.* **2020**, *15*, 6815−6828.
(57) Bard, A. J.; Faulkner, L. R. *Electrochemical Methods: Fundamentals and Applications*; John Wiley: New York, 2001.
(58) Pause, L.; Robert, M.; Savéant, J.-M. Can Single-Electron Transfer Break an Aromatic Carbon−Heteroatom Bond in One Step? A Novel Example of Transition between Stepwise and Concerted Mechanisms in the Reduction of Aromatic Iodides. *J. Am. Chem. Soc.* **1999**, *121* (30), 7158−7159.
(59) Ignaczak, A.; Gomes, J. A. N. F. Quantum Calculations on the Adsorption of Halide Ions on the Noble Metals. *J. Electroanal. Chem.* **1997**, *420* (1), 71−78.
(60) Isse, A. A.; De Giusti, A.; Gennaro, A.; Falciola, L.; Mussini, P. R. Electrochemical Reduction of Benzyl Halides at a Silver Electrode. *Electrochim. Acta* **2006**, *51* (23), 4956−4964.
(61) Ardizzone, S.; Cappelletti, G.; Mussini, P. R.; Rondinini, S.; Doubova, L. M. Adsorption Competition Effects in the Electrocatalytic Reduction of Organic Halides on Silver. *J. Electroanal. Chem.* **2002**, *532* (1), 285−293.
(62) Bellomunno, C.; Bonanomi, D.; Falciola, L.; Longhi, M.; Mussini, P. R.; Doubova, L. M.; Di Silvestro, G. Building up an Electrocatalytic Activity Scale of Cathode Materials for Organic Halide Reductions. *Electrochim. Acta* **2005**, *50* (11), 2331−2341.
(63) Grecchi, S.; Arnaboldi, S.; Isse, A. A.; D'Aloi, C.; Gennaro, A.; Mussini, P. R. Electrocatalytic Reduction of Bromothiophenes vs Bromobenzenes on Gold and Silver Electrodes: Enhancement from S Specific Adsorption and Modulation from Substituent Effects. *Electrochim. Acta* **2022**, *403*, No. 139563.
(64) Saveant, J. M. A Simple Model for the Kinetics of Dissociative Electron Transfer in Polar Solvents. Application to the Homogeneous and Heterogeneous Reduction of Alkyl Halides. *J. Am. Chem. Soc.* **1987**, *109* (22), 6788−6795.
(65) Costentin, C.; Limoges, B.; Robert, M.; Tard, C. A Pioneering Career in Electrochemistry: Jean-Michel Savéant. *ACS Catal.* **2021**, *11* (6), 3224−3238.
(66) Andrieux, C. P.; Savéant, J.-M.; Tallec, A.; Tardivel, R.; Tardy, C. Concerted and Stepwise Dissociative Electron Transfers. Oxidability of the Leaving Group and Strength of the Breaking Bond as Mechanism and Reactivity Governing Factors Illustrated by the Electrochemical Reduction of α-Substituted Acetophenones. *J. Am. Chem. Soc.* **1997**, *119* (10), 2420−2429.
(67) Tavernier, H. L.; Barzykin, A. V.; Tachiya, M.; Fayer, M. D. Solvent Reorganization Energy and Free Energy Change for Donor/Acceptor Electron Transfer at Micelle Surfaces: Theory and Experiment. *J. Phys. Chem. B* **1998**, *102* (31), 6078−6088.
(68) Mewes, J.-M.; You, Z.-Q.; Wormit, M.; Kriesche, T.; Herbert, J. M.; Dreuw, A. Experimental Benchmark Data and Systematic Evaluation of Two a Posteriori, Polarizable-Continuum Corrections for Vertical Excitation Energies in Solution. *J. Phys. Chem. A* **2015**, *119* (21), 5446−5464.
(69) Andrieux, C. P.; Le Gorande, A.; Saveant, J. M. Electron Transfer and Bond Breaking. Examples of Passage from a Sequential to a Concerted Mechanism in the Electrochemical Reductive Cleavage of Arylmethyl Halides. *J. Am. Chem. Soc.* **1992**, *114* (17), 6892−6904.
(70) Costentin, C.; Robert, M.; Savéant, J.-M. Electron Transfer and Bond Breaking: Recent Advances. *Chem. Phys.* **2006**, *324* (1), 40−56.
(71) Andrieux, C. P.; Differding, E.; Robert, M.; Saveant, J. M. Controlling Factors of Stepwise versus Concerted Reductive Cleavages. Illustrative Examples in the Electrochemical Reductive Breaking of Nitrogen-Halogen Bonds in Aromatic N-Halosultams. *J. Am. Chem. Soc.* **1993**, *115* (15), 6592−6599.
(72) Camdzic, D.; Dickman, R. A.; Aga, D. S. Total and Class-Specific Analysis of per- and Polyfluoroalkyl Substances in Environmental Samples Using Nuclear Magnetic Resonance Spectroscopy. *J. Hazard. Mater. Lett.* **2021**, *2*, No. 100023.
(73) Wang, Z.; Jin, X.; Hong, R.; Wang, X.; Chen, Z.; Gao, G.; He, H.; Liu, J.; Gu, C. New Indole Derivative Heterogeneous System for the Synergistic Reduction and Oxidation of Various Per-/Polyfluoroalkyl Substances: Insights into the Degradation/Defluorination Mechanism. *Environ. Sci. Technol.* **2023**, *57* (50), 21459−21469.
(74) Zhao, H.; McMillan, A. J.; Constantin, T.; Mykura, R. C.; Juliá, F.; Leonori, D. Merging Halogen-Atom Transfer (XAT) and Cobalt Catalysis to Override E2-Selectivity in the Elimination of Alkyl Halides: A Mild Route toward Contra-Thermodynamic Olefins. *J. Am. Chem. Soc.* **2021**, *143* (36), 14806−14813.